

Thermal and Mechanical Analysis of PM Assisted Synchronous Reluctance Motor for Washing Machines

Liridon Xheladini, Alper Tap, Murat Imeryuz, Tasdemir Asan, Murat Yilmaz, Lale T. Ergene

Electrical Engineering Department, Istanbul Technical University 34469 Istanbul, Turkey
djeladini@itu.edu.tr, tap@itu.edu.tr, imeryuz@itu.edu.tr, asan@itu.edu.tr, myilmaz@itu.edu.tr, ergenel@itu.edu.tr

Abstract

In this paper, a sample Permanent Magnet Assisted Synchronous Reluctance Motor (PMaSynRM) designed for washing machine applications is analyzed thermally and mechanically. Since washers operate at two different modes, washing and spinning modes, both analyses have been done for the two operating conditions. First of all, referring to the electro-magnetic characteristics of the sample motor, input current, copper losses, iron losses and output torque for both operating modes have been observed. Using these parameters, analytical thermal model for the motor is developed in Motor-CAD and analyzed. Considering the disadvantages of the sample motor performance at steady-state temperatures, the motor is further optimized and analyzed thermally and electromagnetically in the same way as the sample motor. Following the thermal analysis, mechanical analysis is performed using static structural module of ANSYS. Mechanical analysis is also performed for both motors at both operating conditions to see which one is better in mechanical aspect.

Keywords— Heat Transfer, Thermal Circuit, Steady-state Temperatures, Transient Temperatures, Equivalent Stress, Equivalent Strain, Total Deformation.

1. Introduction

The majority of the operational limitations in electrical machines are determined according to the thermal restraints of its components. The most critical of all thermal limitations is the maximum winding temperature that the machine can withstand under constant load operation. Exceeding the thermal boundary of the windings, halves the lifetime of the machine for every 10 °K above the limit [1]. The failures that occur in electrical machines due to violation of thermal limits include oxidation of the copper wire insulation material, demagnetization of permanent magnets (PM), change in the lubrication oil and mechanical expansion. Change of the lubricator and mechanical expansion generally results in bearing failure. Statistically, winding and bearing failures make up about 80% of all electrical machine failures [2]. Therefore, one of the most important stages of an electrical motor design is its thermal analysis. In literature, there are two different thermal models of electric motors used in such analysis. First one are the models that use finite element methods (FEM). Such models perform thermal analysis by dividing the motor geometry into small parts and solving the heat transfer

equations for each part. However, this method requires high data storage capabilities and its calculations last for long periods. The second method includes analytical solutions of thermal circuits defined by dividing the motor in several parts. Each of these parts correspond to a node where the temperature is going to be measured. In literature, several types of high speed electric motors studied, have shown good performances in different applications [3-6]. PMaSynRMs are being used more and more in such high speed applications. The majority of the active losses in PMaSynRM occur in stator windings. Calculating the temperature values of the windings, the insulation class should be chosen accordingly so that the motor will operate for longer times without damaging the winding insulation. In order to keep the temperature values inside an electric motor within pre-defined limits, different cooling methods like natural convection, self-ventilation cooling, housing water jackets, wet rotor, spray cooling and radiation can be applied [7].

2. Sample PMaSynRM

The sample motor is a 4 pole/36 slot, whose geometry is given in Figure 1. The PMs are placed in the first barrier on the d-axis for this sample rotor. Rotor has three flux barriers employing a q-axis insulation ratio of 0.9 and d-axis insulation ratio of 1. The speed-torque characteristics of the sample motor are obtained in Motor-LAB module, with a maximum peak phase current of 3 A and a 311V DC link voltage inverter. Other characteristics of the sample motor are given in Table 1.

Table 1. Characteristics of the sample motor.

Turns/phase	420
Phase resistance (Ohms)	6.7
Air gap(mm)	1
Outer diameter(mm)	120
Magnet volume(cm3)	19.16

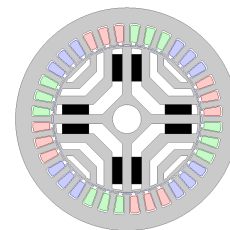


Fig. 1. Cross sectional view of the sample motor.

Using the speed-torque characteristics of the motor, the current and the load angle for both operating conditions are recorded, and the corresponding losses are obtained by simulating each mode separately, as given in Table 2. The magnetic flux density for washing and spinning modes are given in Figure 2.

Table 2. Ratings and losses of the sample motor at 20 °C.

Operation Mode	Washing	Spinning
Speed (min ⁻¹)	563	13000
Current (A)	2	1.2
Torque (Nm)	1.25	0.3
DC Copper losses (W)	79.63	28.36
Iron losses (W)	0.9	15.74

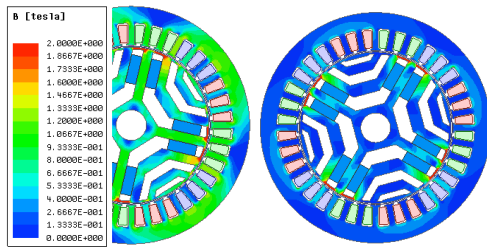


Fig. 2. Magnetic flux density distributions of the sample motor for washing and spinning modes at any instant of time.

Since the motor is designed for washers, it operates at two different modes, washing and spinning operating modes. The sample motor ratings and the losses at 20 °C for the given operating modes are given in Table 2.

3. Thermal Analysis of the Sample Motor

It is accepted that the development and the high accuracy of the thermal models of electric motors is more difficult than their electromagnetic models [7]. In Motor-CAD, instead of importing motor drawings from another software, the thermal model of the motor is obtained by changing several numerical parameters defined in the software interface. Using the geometry dimensions and the data given in Table 1, the thermal model of the sample motor is developed as follows.

3.1. Loss Settings

Winding resistance increases proportionally to temperature. Therefore, to get a better analysis for the motor performance at steady state temperatures, iterative solutions between electro-magnetic and thermal modules of Motor-CAD are done until solutions of both modules converge to constant values. At steady-state temperature the phase resistance of the motor becomes 10.39 ohms and the active losses increase to 124.8 W. The iron losses do not change too much with temperature, therefore the same value of iron losses given in Table 2 is used for completing the loss settings.

3.2. Geometry Settings

The geometry settings and the defined geometry is given in Figure 3. The stator of the sample motor defined

in Motor-CAD is exactly the same as the geometry defined in Maxwell 2D FEM Analysis Software. However, as a result of limited parameter number in the rotor side, the defined geometry is an approximation of the original one. The magnet length is changed by a single parameter, therefore, the magnet volume in the Motor-CAD geometry is distributed in three barriers with the same ratio as in the original geometry.

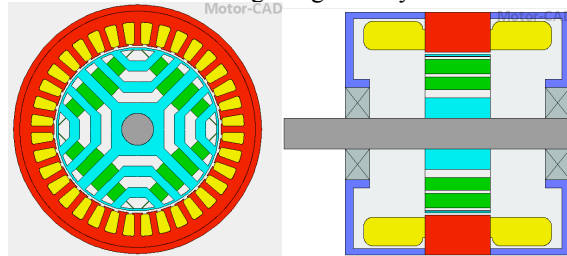


Fig. 3. Radial and axial view of the sample motor in Motor-CAD.

3.3. Winding Settings

In the winding settings, the available parameters include the winding type, slot fill factor and conductor diameter. In the performed analysis, the conductor number/slot is chosen as 70. "Ewdg MLT" factor defined the ratio of the winding length that remains outside the stack length. Since the motor's stack length is small and the winding is distributed, the end-winding mean length is calculated and inserted in the winding settings. The conductor configuration in a single slot and the corresponding settings are given in Figure 4.

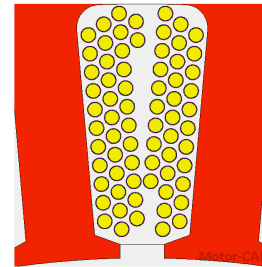


Fig. 4. Single slot winding configuration of the sample motor.

3.4. Material Settings

The thermal properties of the materials used in thermal analysis are given in Table 3.

Table 3. Active used materials and their thermal properties

Materials	Thermal Conductivity [W/m/ °C]
M700	30
Aluminium	168
Copper	401
Ferrite	4
Mild Steel	25

3.5. Front and Rear End-Space Settings

In the front and rear end-spaces of the motor, air flow occurs due to the rotation of the rotor. The parameter that affects the air motion in end-space is the type of the rotor

which is defined in end-space settings. In this analysis, the type of the rotor is selected to be normal one, with a medium end-space velocity multiplier. According to the rotor type, the software calculates a reference air speed on the end-spaces, and using this reference speed, for all the motor parts separately that are in contact with the end-space air, it calculates the air speed flowing around them. To calculate the air speed around each part in the end-spaces, the software uses k_1 , k_2 and k_3 constants. Using these constants, the heat transfer factor in the end-space (h), is calculated using the reference air speed with the following equation:

$$h = k_1 \times [1 + k_2 \times vel] \times k_3 \quad (1)$$

In equation (1), “ vel ” is the reference speed in the end-space. This reference speed is only used for the stationary parts of the motor. The air speed around the rotation parts is calculated according to their rotational velocity and their average distance(radius) from the shaft center. Different researches give different values for the, k_1 , k_2 and k_3 constants. However, all researches give similar results while implementing the thermal circuit of the motor. In the Scuber’s researches, the constants used for induction motor thermal analysis are $k_1=15$, $k_2=0.4$ and $k_3=0.9$ [8]. Because induction motor end-space is similar to the synchronous reluctance motor end-space, the same constants are used in this model’s thermal analysis also. The endcaps are completely closed, therefore endcap ventilation is selected as closed. Details for the front and rear end-space settings are given in Figure 5 and 6, respectively.

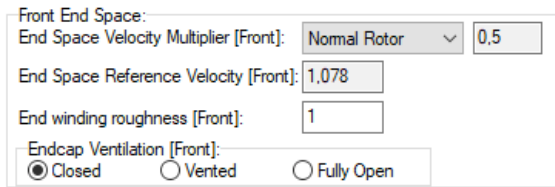


Fig. 5. Front end space settings.

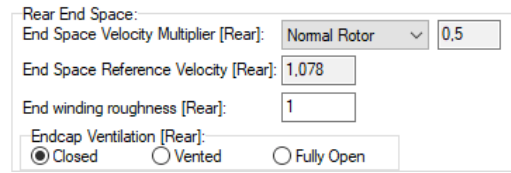


Fig. 6. Rear end space settings.

3.6. Thermal Results of Washing Mode Operation

After the settings related to the thermal model are finished, the software implements the thermal circuit corresponding to the model giving the temperature results at each node of the motor. As it was expected, the maximum thermal stress occurs in the stator windings. Referring to the thermal circuit, radial and axial view of the motor, it can be concluded that the maximum temperature value seen in the stator is $152.4\text{ }^{\circ}\text{C}$, whereas the maximum winding temperature is $164.2\text{ }^{\circ}\text{C}$. Figure 7 gives the thermal circuit implemented by the software and all the node temperature of the motor.

3.7. Thermal Results of Spinning Mode Operation

At spinning mode, the speed of the motor reaches up to 13000 min^{-1} for short periods of time. These periods do not last longer than 3 minutes, therefore the following transient analysis includes a washing mode period of 10000 sec followed by a 3 min period of spinning mode.

The transient change of the winding and stator lamination temperatures are given in Figure 8. During the spinning mode operation, since the copper losses are lower, the winding temperature drops near to $155\text{ }^{\circ}\text{C}$ for period of 3 minutes.

After the speed is decreased again to washing mode speed of 563 min^{-1} , losses and temperatures start rising again to the previously calculated washing mode values.

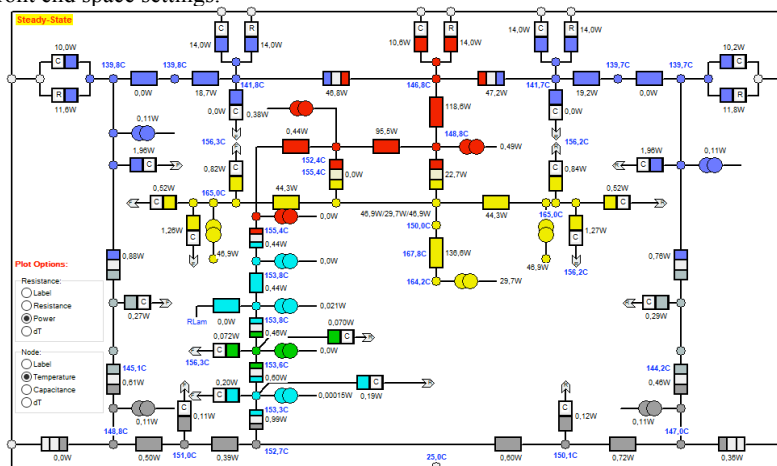


Fig. 7. Equivalent thermal circuit of the sample mot

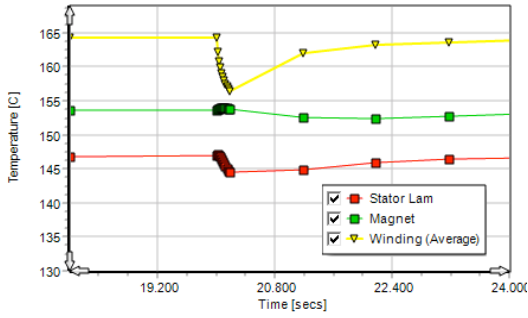


Fig. 8. Transients of the winding, magnet and stator lamination temperatures during spinning mode operation.

3.8. Demagnetization of ferrites due to temperature rise

The temperature of the ferrite magnets at steady state operation, as can be seen from thermal circuit in Figure 10, reaches a temperature of 153.61 °C. This temperature value of the magnet, causes the remanent flux density to decrease from 0.379T to 0.291T. Thus, the maximum torque that the motor can induce becomes 1.11 Nm. Therefore, this design becomes problematic and disadvantageous at high temperatures. Thermal analysis results, show that further optimization of the motor is required.

4. Optimized PMaSynRM Motor Electro-Magnetical Characteristics

Keeping the outer radius, pole and slot number of the motor same, the air-gap and the number of turns per phase are changed in the optimized motor. Its cross sectional view is given in Figure 9. On the rotor side, the d and q-axis insulation ratios are equal to those of sample motor, and the magnet location is the side of the first flux barrier.

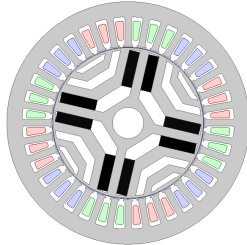


Fig. 9. Cross sectional view of the optimized motor.

General characteristics of the optimized motor are given in Table 4.

Table 4. Optimized motor properties.

Turns/phase	450
Phase resistance	5.37
Air gap(mm)	0.8
Outer diameter(mm)	120
Magnet volume(cm3)	23

The washing and spinning mode characteristics of the sample motor are obtained in Motor-LAB module, with a maximum peak phase current of 3 A and a 311 V DC link voltage of the inverter. The ratings of the motor for

washing and spinning mode operations at 20°C are recorded and given in Table 5.

Table 5. Ratings and losses of the optimized motor at 20°C.

Operation Mode	Washing	Spinning
Speed(min ⁻¹)	563	13000
Current(A)	1.62	1.3
Torque(Nm)	1.25	0.3
DC Copper losses(W)	42.3	27.44
Iron losses(W)	1.06	29.22

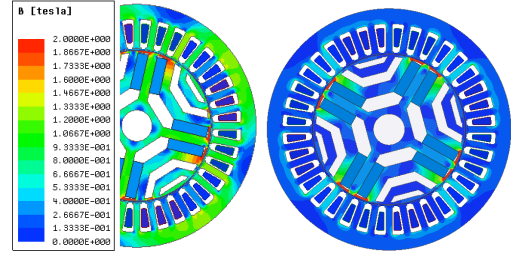


Fig. 11. Magnetic flux density distributions of the optimized motor for washing and spinning modes at any instant of time.

Similar to the sample motor, to have a better view on how the field is weakened at spinning mode, the flux densities of the optimized motor for both operations are given in Figure 11.

5. Thermal Analysis of the Optimized Motor

Similar to the previous motor, iterative solution between the thermal and electromagnetic model of the optimized motor is provided to have a better view on the performance of the motor at high temperatures. From the radial view of the thermal model solution, given in Fig. 12, it can be see that the winding temperature rises up to 98.3°C, causing the phase resistance, at steady-state, to change to 7.12 ohms. The active losses increase also to 55.96 W. The iron losses do not change too much with temperature, therefore the same value of iron losses given in Table 5 are used for completing the loss settings. On the other hand, the magnet temperature increases up to 94.6°C. This steady state temperature causes the remanent flux density of the ferrite magnets to drop from 0.397T to 0.336T. The maximum torque that the motor can induce becomes 1,19Nm at the same input current. Considering the transient operation at spinning mode, since the current is lower than washing mode, the copper losses are lower, therefore the winding temperature will drop.

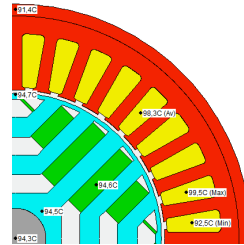


Fig. 12. Cross sectional view of the temperature values of the optimized motor.

6. Mechanical Analysis

Mechanical analysis of high speed motors is another important issue to be considered during motor designs. In order to determine whether the motor's mechanical integrity will be sustained, in this section the stress analysis of the sample and optimized motors are simulated in ANSYS. The simulations are performed separately for washing (563 min⁻¹) and spinning mode (13000 min⁻¹) for both models. The mechanic characteristics of the materials composing the rotor are given in Table 6.

Table 6. Mechanical Characteristics of the materials

Parameters	M700	Ferrite
Mass density [kg/m ³]	7800	5000
Young modulus [GPa]	210	180
Poisson coefficient	0.31	0.28
Tensile stress limit [MPa]	405	34

6.1. Washing Mode Test

The mechanical test during washing mode is performed to see the total deformation and the equivalent stress on the rotor under constant torque of 1.25 Nm. The simulations and results for total deformation of sample and optimized motor are given in Figure 13.

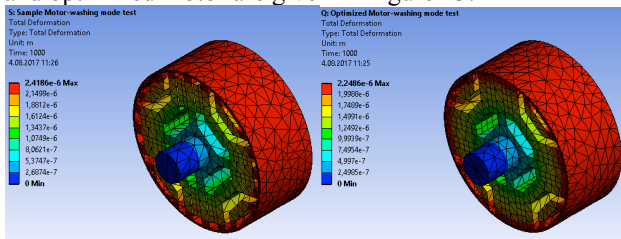


Fig. 13. Total deformation of the sample and optimized motors for the washing mode.

6.2. Spinning Mode Test

The mechanical test during spinning mode is performed to see the total deformation and the equivalent stress on the rotor under constant rotational speed of 13000 min⁻¹. The simulations and results for total deformation of sample and optimized motor are given in Figure 14.

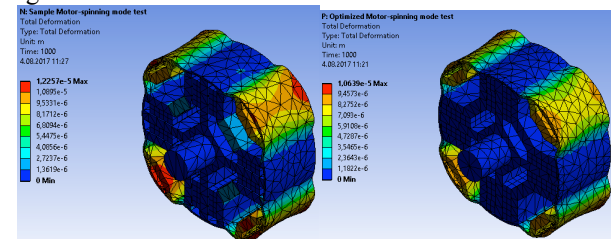


Fig. 14. Total deformation of the sample and optimized motors for the spinning mode.

7. Conclusion

The final results of the thermal analysis are given in Table 7. Looking at the maximum values of winding temperatures of both motors, it is clearly seen that the

sample motor undergoes larger thermal stresses than the optimized motor. Its insulation class of the winding is required to be H class that can withstand temperatures up to 180 °C. Moreover, high temperatures also decrease the remanent flux of the ferrite magnets, causing the torque capability of the motor to drop drastically. On the other hand, the optimized motor has much lower losses and it undergoes lower thermal stresses during steady-state operation. Insulation class A, withstanding temperatures up to 105 °C, is enough for this motor. Also, the torque capability of the motor does not drop much at steady state operation temperatures.

Table 7. Ratings and losses of optimized motor at 20 °C.

Model	Sample Motor	Optimized Motor
Max. Winding Temp.(°C)	164.2	98.3
Isolation class	H	A
Magnet Temp.(°C)	153.6	96.59
Ferrite Br.(T)	0.291	0.336
Torque(Nm)	1.11	1.19

Referring to the mechanical analysis results, glue that is used between the magnets and the ferromagnetic material has a significant positive effect on the rotor deformation. Making the rotor more compact, the stresses and the maximum deformation are reduced. Moreover, from the mechanical results in Table 8 it is clearly seen that the optimized motor is advantageous also in mechanical aspect. Larger magnets and smaller rotor radius, makes the optimized motor's rotor better than the sample motor. Maximum deformation of the optimized motor 10.64 μm, which is negligibly small.

Table 8. Mechanical results at 20 °C.

Model Test	Sample Motor		Optimized motor	
	Spinning	Washing	Spinning	Washing
Stress (MPa)	96.04	3.31	105.45	3.2
Elastic strain (m/m)	0.0005	15.830E-06	0.00052	15.24E-06
Total deform. (μm)	12.26	2.42	10.64	2.25

Acknowledgment

This work was supported by the Scientific and Technological Research Council of Turkey (TUBITAK) with the Grant No: 115E416 and ITU Research Funding Grant No: ITU-BAP-39466. The authors would also like to thank Dr. David STATON at Motor Design Ltd.

8. References

- [1] Sadarangani Ch., Electrical Machines - Design and Analysis of Induction and Permanent Magnet Motors., Division of Electrical Machines and Power Electronics School of Electrical Engineering, KTH.
- [2] "Induction machine on-line condition monitoring and fault diagnosis – a survey" Baldor Corporation
- [3] N. Bianchi, S. Bolognani, and F. Luise, "Potentials and Limits of HighSpeed PM Motors", IEEE Trans. on Indus. Appl., vol. 40, no. 6, pp. 1570- 1578, Nov/Dec. 2004.
- [4] A. Binder, T. Schneider, and M. Klohr, "Fixation of Buried and Surface Mounted Magnets in High-Speed Permanent-Magnet Synchronous Machines", IEEE Trans. on Indus. Appl., vol. 42, no. 4, pp. 1031-1037, July/Aug. 2006.
- [5] S-I. Kim, Y-K. Kim, G-H. Lee, and J-P. Hong, "A Novel Rotor Configuration and Experimental Verification of Interior PM Synchronous Motor for High-Speed Applications", in IEEE Trans. on Magn., vol. 48, no. 2, pp. 843-846, Feb. 2012.

- [6] A. Gilson, S. Tavernier, M. Gerber, C. Espanet, F. Dubas, and D. Depernet, "Design of a Cost-Efficient High-Speed High-Efficiency PM Machine for Compressor Applications", in Proceed. of Ener. Conv. Cong. and Expo. (ECCE), Montreal, 20-24 Sep. 2015.
- [7] Staton D., Hawkins D., Popescu M., "Thermal Behaviour of Electrical Motors – An Analytical Approach", Motor Design Ltd., Ellesmere, SY12 0EG, U.K.
- [8] "MotorCAD User Manual", Motor Design Limited, 2016, Ellesmere, U.K.